

Old open clusters: the interesting case of Berkeley 21^{*}

M. Tosi¹, L. Pulone^{2,3}, G. Marconi², A. Bragaglia¹

¹ *Osservatorio Astronomico di Bologna, Italy, e-mail angela@astbo3.bo.astro.it, tosi@astbo3.bo.astro.it*

² *Osservatorio Astronomico Roma – Monte Porzio, Italy, e-mail pulone@coma.mporzio.astro.it, marconi@coma.mporzio.astro.it*

³ *European Southern Observatory, Garching bei München, Germany, lpulone@eso.org*

ABSTRACT

We present CCD BVI photometry of the old open cluster Berkeley 21, one of the most distant clusters in the Galactic anticentre direction, and possibly the lowest metallicity object in the open clusters sample. Its position and metal abundance make it very important for the study of the Galactic disc.

Using the synthetic Colour - Magnitude Diagram method, we estimate values for distance modulus $(m-M)_0 = 13.4\text{--}13.6$, reddening $E(B-V) = 0.74\text{--}0.78$ (with possible differential absorption), and age = 2.2–2.5 Gyr.

Key words: Hertzsprung-Russell (HR) diagram – open clusters and associations: general – open clusters and associations: individual: Berkeley 21

1 INTRODUCTION

Old open clusters cover a large range of distances, metallicities, and ages (Friel 1995), and that warrants their use in investigations of the chemical and dynamical evolution of our Galaxy. To study the metallicity and age distribution of open clusters with Galactocentric distance, and avoid unnecessary and dangerous biases, a key requisite is homogenous analysis of very accurate observational data, as discussed by, e.g. Janes & Phelps (1994, JP94) Carraro & Chiosi (1994, CC94), Friel (1995), Twarog et al. (1997, TAAT97).

This is the fifth paper of a series dedicated to the examination of old open clusters of different ages and metallicities, and located at different Galactic radii: for them we measure in a homogenous way distance, age, reddening and metallicity. These quantities are derived from comparison of the observed colour-magnitude diagrams (CMDs) to synthetic ones generated by a numerical code based on stellar evolution tracks and taking into account theoretical and observational uncertainties (Tosi et al. 1991). These simulations are much more powerful than the classical isochrone fitting method to study the evolutionary status of the analysed region and have been successfully applied both to nearby irregular galaxies (Greggio et al. 1998 and references therein) and to galactic open clusters (NGC2243: Bonifazi et al. 1990; Cr261: Gozzoli et al. 1996; NGC6253: Bragaglia et al. 1997; NGC2506: Marconi et al. 1997).

Berkeley 21 (Be21) is located toward the Galactic anticentre, at coordinates $RA(1950) = 5:48:42$, $DEC(1950) = 21:46$, and $l_{\text{II}} = 187^\circ$, $b_{\text{II}} = -2.5^\circ$. It has already been observed by Christian & Janes (1979, hereafter CJ), but

their photographic CMD is very shallow, barely reaching the main sequence Turn-Off (TO). They deduced a substantial reddening ($E(B-V) \simeq 1.0$), a large distance modulus ($(m-M)_0 \simeq 16$), and a quite young age ($\sim 10^8$ yr). Much better data have been presented by Phelps et al. (1994, PJM94) in their compilation of old open clusters, providing $(m-M)_0 = 13.9 \pm 0.2$ and an age of 2.8 Gyr, derived on the basis of $\delta V = 1.6$ (δV being the magnitude difference between TO and clump stars, JP94). The metallicity has been estimated by medium-resolution spectroscopy (Friel & Janes 1993, FJ93), but its actual value strongly depends on the adopted reddening ($E(B-V) = 0.7 \pm 0.2$, Janes 1991), with $[Fe/H] = -0.97_{-0.1}^{+0.3}$ dex. This large uncertainty, given the fact that Be21 defines the lowest metallicity limit of the open clusters sample and is one of the clusters most distant from the Galactic centre, is a further limitation for studies of the (possible) age and distance relations with chemical abundance in the Galactic disc (see also Twarog et al. 1997).

In Section 2 we describe the observations and data analysis; in Section 3 we present the derived CMDs involving BVI photometry and discuss the presence of binary stars. In Section 4 we compare observed and synthetic CMDs and derive metallicity, age, distance and reddening. Finally, conclusions will be reviewed in Section 5.

2 OBSERVATION AND DATA REDUCTIONS

Be21 was observed at the 1.54m Danish telescope located in La Silla, Chile, on March 4-5, 1995; the field was centered on the cluster. The direct camera mounted the CCD #28, a Tek 1024×1024, with a scale of 0.377 arcsec/pix, yielding a field of view of 6.4×6.4 arcmin². The observed region is

^{*} Based on observations made in La Silla, ESO

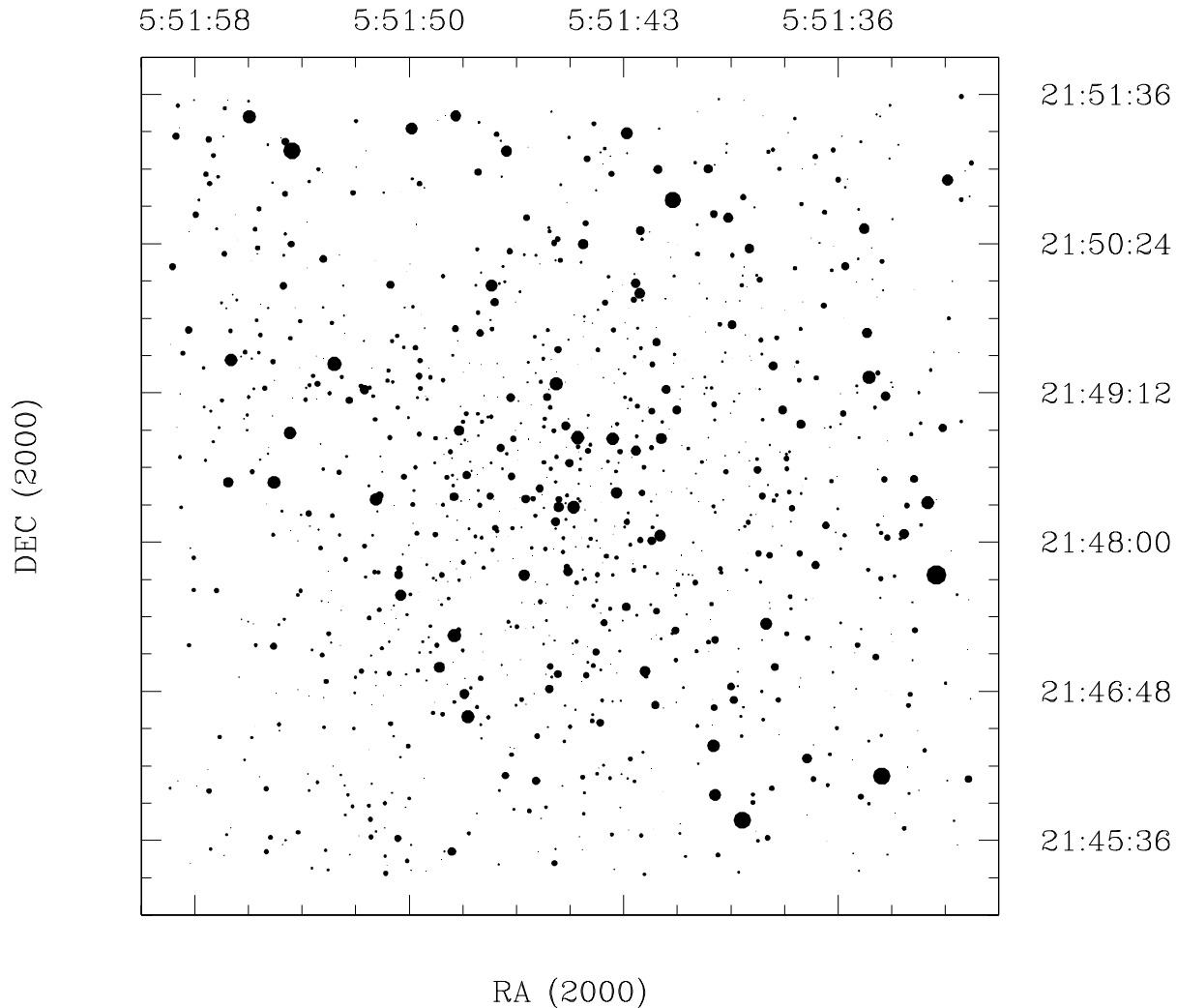


Figure 1. Map of the observed field, taken from our $V, B - V$ photometry. North is up and East left.

Table 1. Log of the observations. The cluster field has its centre at $RA(2000) = 5:51:46$, $DEC(2000) = +21:48:45$. The off-cluster field has coordinates: $RA(2000) = 5:52:08$, $DEC(2000) = +21:53:53$

Night	Field	Tel.	Exposure in seconds			Seeing excursion
			B	V	I	
Mar 4	Centre	Danish	120	120	120	0.90-1.20
Mar 4	Centre	Danish	-	120	900	0.85-1.00
Mar 4	Centre	Danish	-	600	-	0.95-1.10
Mar 5	Centre	Danish	120	120	120	1.00-1.10
Mar 5	Centre	Danish	1500	900	-	0.95-1.10
Mar 14	Ext.	Dutch	120	60	60	1.10-1.30
Mar 14	Ext.	Dutch	1200	480	480	1.20-1.30
Mar 14	Ext.	Dutch	1200	480	480	1.15-1.30

shown in Fig. 1, derived from our photometry (bright field stars may be missing), and oriented with North up and East left. At least one of the two nights (March 5) was photometric, while cirri were occasionally present during the other.

Seeing conditions were quite good for the site/telescope and the seeing excursion for each night is given in Table 1, together with a list of exposures. A second adjacent area, to be used for field decontamination, was observed with the 0.91m Dutch telescope, also in La Silla, a few days later. In this case the field of view is of 3.8×3.8 arcmin².

Standard CCD reduction of bias and dark current subtraction, trimming, and flatfield correction were performed. We applied to all frames the usual procedure for PSF study and fitting available in DAOPHOT-II (Stetson 1992) in MIDAS environment. The deepest I frame of each field has been used to search for stellar objects, setting the minimum photometric threshold for object detection at 3σ above the local sky background. The objects identified in the I band were then fitted in all the others.

The formal errors as given by DAOPHOT are quite small: they range from 0.005 mag for $V < 17$ to 0.04 at $V \simeq 22$, from 0.001 mag for $B < 18$ to 0.08 at $B \simeq 22$, and from 0.005 for $I < 17$ to 0.07 at $I \simeq 22$. The circumstance that the synthetic CMDs described in Sect. 4 reproduce quite well the observed stellar spread in the diagram when adopting these formal errors, guarantees that even if they do underestimate

Table 2. Comparison between our magnitudes and the ones in CJ for the 8 stars in common. The differences in columns 5 and 6 are in the direction of our values minus CJ’s.

N_{CJ}	V_{CJ}	$(B - V)_{CJ}$	N	ΔV	ΔB
250	12.80	0.92	1105	-0.081	-0.060
254	13.53	1.27	1106	0.054	0.063
14	13.75	0.74	26	-0.050	-0.048
260	13.65	0.87	7	0.040	0.056
211	15.10	1.43	97	0.092	0.054
90	15.32	0.93	93	0.022	0.015
227	15.46	0.88	57	0.045	0.026
168	16.88	1.42	115	-0.061	-0.043

the actual size of the photometric errors, the difference must be quite small, thanks to the good seeing and relatively uncrowded conditions of these data.

Finally, aperture photometry was performed on a few isolated stars (of which 7 were eventually retained) in all images, to compute a correction to the PSF derived magnitudes and be on the same system as the photometric standard stars. An indication of the good fit obtained for the PSF of each frame is that this correction is always small, being of a few hundredths of magnitude in most fields, and barely reaching 0.1 mag in the very worst cases.

2.1 Photometric calibrations

The conversion from instrumental magnitudes to the Johnson-Cousins standard system was obtained using a set of primary calibrators (Landolt 1992) which spanned a wide range in colour ($-0.287 \leq B-V \leq +1.147$). Standard stars fields were analysed using aperture photometry. The calibration equations were derived using the extinction coefficients for La Silla taken from the database maintained by the photometric group at the Geneva Observatory Archive. We obtained equations in the form:

$$B = b + 0.206(\pm 0.021) \cdot (b - v) - 4.135(\pm 0.018)$$

$$V = v + 0.021(\pm 0.010) \cdot (b - v) - 3.916(\pm 0.009)$$

$$V = v + 0.000(\pm 0.014) \cdot (v - i) - 4.011(\pm 0.015)$$

$$I = i - 0.013(\pm 0.011) \cdot (v - i) - 4.069(\pm 0.010)$$

where b, v, i are instrumental magnitudes, while B, V, I are the corresponding Johnson-Cousins magnitudes. The V values have been obtained from the equation involving the $b-v$ colour for all stars found and measured in the B frame (1138 objects), and from the one involving the $v-i$ colour for the remaining 429 objects. The two calibrations are similar for the stars in common, without offsets or trends. We calibrated in each filter the March 5 data using these equations and later used them to extend the calibration to all the other exposures.

We have 8 stars in common with the photoelectric observations in CJ, and the comparison looks good, with no indications of systematic errors in our photometry: the difference in V magnitude is always less than 0.1 mag, and

Table 3. Completeness of our measurements. Each value is the average of 5 trials for B, and 3 trials for V and I. For each magnitude bin, 10 % of the total number of stars were added, following the luminosity function.

Mag interv.	%B	%V	%I
< 19.0	100	100	100
19.0-19.5	100	100	95
19.5-20.0	100	100	80
20.0-20.5	100	100	29
20.5-21.0	100	98	10
21.0-21.5	100	78	
21.5-22.0	100	69	
22.0-22.5	89	14	
22.5-23.0	66	2	
23.0-23.5	39		
23.5-24.0	11		
24.0-24.5	2		

even better in B (see Table 2), with a mean difference in both cases of only 0.008 mag. No comparison has been attempted with the photographic values in CJ, given the very sparse appearance of the diagram.

2.2 Completeness analysis

We tested the completeness of our luminosity function in the B, V and I band, using the routine ADDSTAR in DAOPHOT-II. In short, we added to the original deepest frames in each filter a pattern of artificial stars, distributed in colour as the real ones ($\simeq 10\%$ of the total in each magnitude bin), at random positions. The obtained “artificial frames” were reduced using exactly the same procedure and the same PSF used for the original images. We considered as “recovered” only those stars found in their given position and magnitude bin. The completeness was then derived as the ratio $N_{recovered}/N_{added}$ of the artificial stars generated. We performed 3 or 5 trials per band, depending on the stability of the results, and the final averaged results are reported in Table 3.

3 THE COLOUR-MAGNITUDE DIAGRAMS

The final sample comprises 1567 stars; of them, 1138 have been measured in all the three bands, while 429 have only V and I values. The complete table with magnitudes and positions is available electronically from the first author. We have given positions both in pixel and in equatorial coordinates. The transformation has been carried out identifying 45 stars well distributed in the field on the Digitized Sky Survey[†] images; we are confident of its precision for the central part of the field, while there might be some distortions (of the order of a few arcsec) near the corners.

Fig. 2 shows our results in the $V, B - V$ and $V, V - I$ planes. The main sequence (MS) appears well delineated

[†] The Digitized Sky Survey was produced at the Space Telescope Science Institute under U. S. Government grant NAG W-2166.

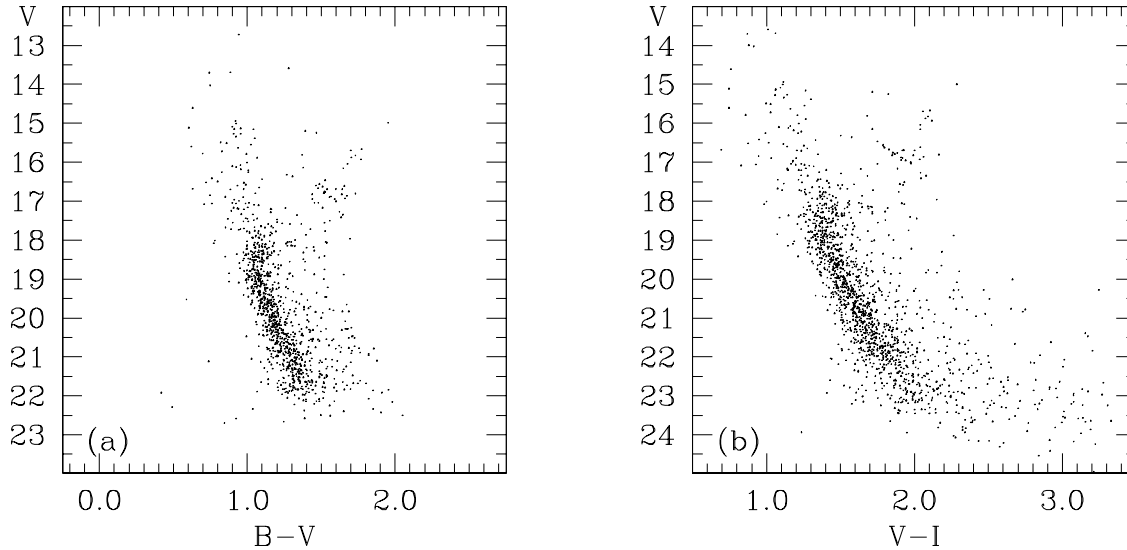


Figure 2. Colour magnitude diagrams for our sample: (a) $V, B - V$ CMD, for 1138 stars, (b) $V, V - I$ CMD for 1567 stars

in both diagrams, and reaches more than four magnitudes fainter than the TO. We estimate for the TO point $V = 18.60$, $B - V = 1.02$ and $V - I = 1.33$. A red clump of objects, which we attribute to core He-burning stars, is present at about $V = 16.80$, $B - V = 1.55$ and $V - I = 1.90$. The sub-giant and red giant branches (SGB, RGB) are also visible, although blurred by field star contamination, considerable especially on the red of the MS.

Our CMDs (Fig. 2) are in agreement with those in PJM94 (their fig. 12); our MS is, however, narrower and 1.5–2.5 mags deeper, thanks to the higher quality data.

We plot in Fig. 3(a)–(d) the $V, B - V$ CMDs at different distances from the centre (assumed at position $X=540$, $Y=520$, or $RA(2000)=5:51:45$, $DEC(2000)=+21:48:20$); the cluster MS is always visible to the image limit. The innermost 1 arcmin region (Fig. 3(a)) appears almost free of field stars, with a narrow MS, and shows presence of blue stragglers stars (BSS). This is valid also for the adjacent region (Fig. 3(b), between 1 and 2 arcmin) while the situation is more difficult to disentangle in the outer rings, where field stars are more numerous.

We note that the BSS seem to be more centrally concentrated than the other cluster stars. If we conservatively define as BSS all the objects brighter than $V=17$, and bluer than $B - V=1.2$, we have 12 of them in the innermost 1 arcmin (as compared to a total of 192 stars), 12 between 1 and 2 arcmin (total 386 stars, and area 3 times larger) and 17 between 2 and 3 arcmin (total 350 stars, and area 5 times larger) with increasing relevance of field stars contamination. The same appears to be true for binary stars: they are almost as many as the single stars at the cluster centre, while their relative relevance decreases outwards (see later).

3.1 Field contamination and differential reddening

To account for field star contamination, we have observed with the Dutch telescope a region off-cluster, about 5.5 arcmin North and East of the cluster centre. The area surveyed by this external field is about 35 % of that covered by the Danish telescope data, and the corresponding $V, B - V$ CMD for the 96 objects found is shown in Fig. 3(e). Taking the area into account, the number of objects expected to be fore/background stars in the cluster $V, (B - V)$ CMD is then about one quarter of the total. Therefore, in the inner 1 arcmin cluster members appear to dominate over the field population: we expect to have only about 20 field stars out of the 192 (cluster plus field) detected objects.

The width of the global MS (Fig. 2) of this cluster appears too large to be explained by field stars and photometric errors, unless we pretend to have underestimated them by more than a factor of ten, which is quite improbable in these photometric conditions. And the presence of a high fraction of binaries (see next section) is also insufficient. On the other hand, the MS width of the central region (Fig. 3(a)) is instead perfectly reproducible (see Sect.4) with the estimated photometric errors when binaries are taken into account. Since the cluster suffers from large and uncertain absorption ($E(B - V) = 0.7 \pm 0.2$, Janes 1991), we have therefore investigated the possibility that there may be differential reddening over its face. We then divided the field in 9 zones of equal area, compared the resulting CMDs, and found that one of the corners is less absorbed than the other parts; the difference in $E(B - V)$ is about 0.1. By changing position and/or size of the zones, we have found that, to a good approximation, we can consider as less reddened the stars in the North-West corner of our field, as shown in Fig. 4(a), where also the central box is indicated for comparison. Fig. 4(b) displays the difference in the CMDs for the central part and the NW corner, and it is apparent that

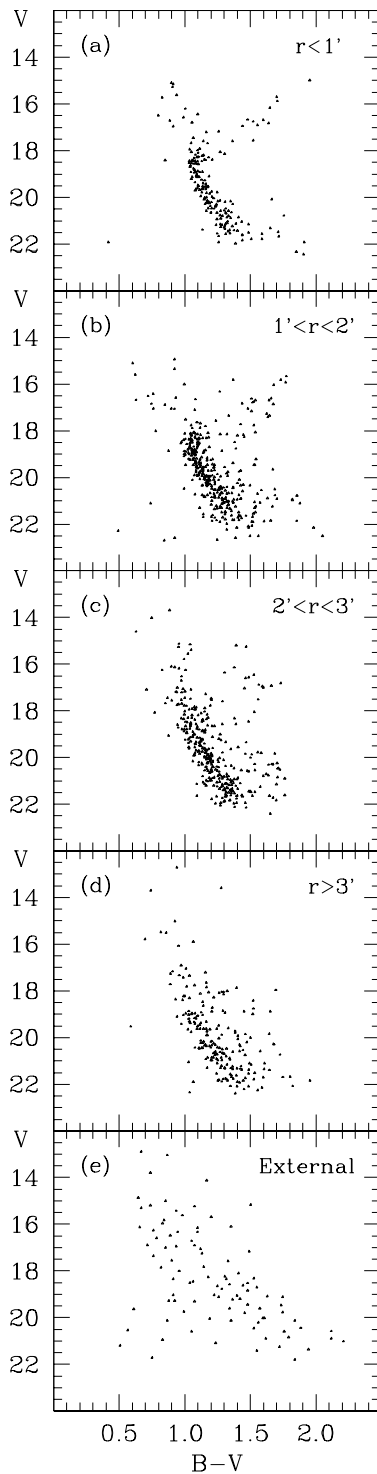


Figure 3. (a) to (d) Radial CMD for Be21; (e) external field. Areas are: 1π , 3π , 5π , 4π , and 4.6π respectively

a significant fraction of the MS width is due to differential reddening.

3.2 Binary stars

At first sight (Fig. 2) searching for binaries doesn't look too promising, given the width of the MS. If one chooses to work with a larger baseline in colour (e.g. $B - I$), the situation improves, but significant results are achieved only when restricting the sample to the very centre of the cluster. After a few trials, we decided to concentrate on the inner 1 arcmin, where differential reddening and field contamination are negligible and the separation between the single and double stars sequences is pretty clear (see Fig. 5(a)). We defined a pseudo MS ridge line (simply joining two points at B about 20 and 22) which fits quite well the single stars MS. To measure the binary population in a more quantitative way, we built the histograms in colour of the stars between $B=20$ and $B=22$, divided in 4 bins half a magnitude wide (Fig. 5(b), where the arrows indicate the position of the "MS ridge line"). It is interesting to notice that binaries seem to outnumber single stars in at least 2 mag bins. To estimate the actual fraction of binaries we have computed the distance of each star in the interval between $B=20$ and $B=22$ from the MS ridge line (Fig. 5(c)). Two peaks are visible, one located around $\Delta(B - I)=0$, which can be considered due to the single stars, and the second, centered at $\Delta(B - I)=0.14$, due to binary stars. We thus deduce a binary fraction of about 45 %. This estimate is based mostly upon systems of stars of near equal mass, that show up well separated from the single-stars MS in the CMD; it is, in this sense, a lower limit to the actual fraction of binaries.

On the other hand, as said above, binaries are likely to be centrally concentrated. This is only a rather qualitative statement, but is also supported by the central concentration of BSS described above. At the cluster centre the single-stars and binary sequences are well separated (see Fig. 5(a)), and there are almost as many objects above and to the red of the single-stars MS than on the MS itself. The situation changes in the adjoining ring, where the picture is blurred by field star contamination, but there appears to be a clustering of stars to the blue of the MS, with decreasing density to the red. The picture is consistent with mass segregation of the more massive objects (MS binaries, BSSs) toward the centre of the cluster.

4 CLUSTER PARAMETERS

To derive the values of the cluster parameters, we have applied to Be21 the approach of CMD simulations described by Tosi et al. (1991) and already employed for four other old open clusters. Due to the existing estimate of the cluster metal content (FJ93), we have restricted the sample of stellar evolutionary tracks adopted to create the synthetic CMDs to the sets with metallicities near that value (i.e. $Z \simeq 0.002$). These sets are summarized in Table 4. For each set of stellar models, we have performed several MonteCarlo simulations for any reasonable combination of age, reddening and distance modulus.

The incompleteness factors and the photometric errors in each magnitude bin assigned to the synthetic stars in each photometric band are those derived from the observed data and described in Sect. 2.

Generally speaking, the CMD of Be21 is not easily reproduceable by stellar models. This is due to the combined

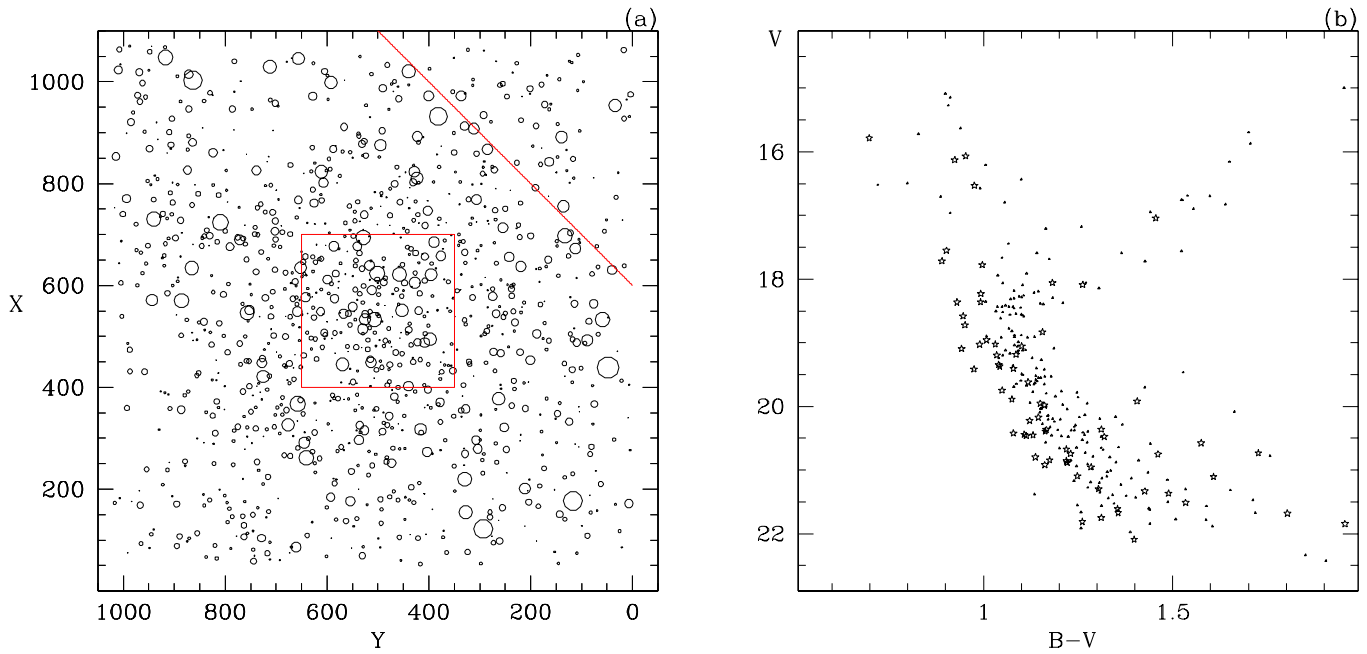


Figure 4. (a) Differential reddening is present over the cluster face: in the upper right corner of our field absorption is less severe. (b) Comparison between the CMD for the upper right corner (star symbols) and the centre of the cluster (dots)

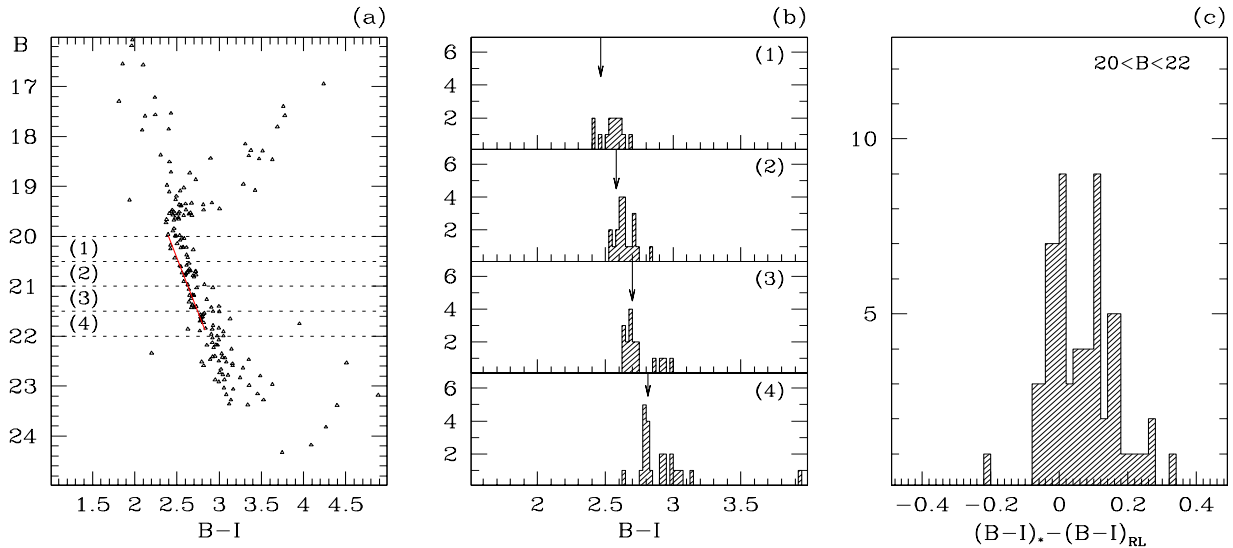


Figure 5. (a) $B, B - I$ CMD (the one with the largest baseline in colour possible with our data). The line is an approximation of the single stars MS ridge line. (b) Histogram in $B - I$ colour for the four different magnitude intervals. The arrows indicate the position of the MS "ridge line" in the middle of each mag bin. (c) Histogram of the difference in colour between stars and the MS "ridge line" shown in (a).

effects of field contamination and differential reddening, to the presence of a large number of blue stragglers candidates and to the underpopulation and/or short extension of the subgiant branch as compared to that expected for a system with the magnitude difference between clump and turnoff

stars observed in Be21. To minimize at least some of these problems in the comparison between observed and simulated CMDs, we have restricted the complete analysis to the inner cluster region where field contamination and reddening variations are not severe. For sake of consistency, we have

Table 4. Stellar evolutionary tracks adopted for the synthetic CMDs

Model	Y	Z	M_{min} (M_{\odot})	M_{max} (M_{\odot})	Reference	Notes
FRANEC	0.27	0.006	0.6	9	Castellani et al. 1993	to AGB-tip, LAOL op.
FRANEC98	0.23	0.001	0.7	9	Straniero, priv.comm.	to AGB-tip, OPAL op.
FRANEC98	0.26	0.006	0.7	9	Straniero, priv.comm.	to AGB-tip, OPAL op.
FRANEC98	0.27	0.010	0.7	9	Straniero, priv.comm.	to AGB-tip, OPAL op.
Geneva	0.24	0.004	0.8	120	Charbonnel et al. 1993	only to RGB-tip
Geneva	0.24	0.001	0.8	120	Schaller et al. 1992	Charbonnel et al. 1996 for e-AGB
Padova	0.24	0.004	0.6	120	Fagotto et al. 1994	to AGB-tip
Padova	0.25	0.008	0.7	120	Alongi et al. 1992	to AGB-tip

also made some simulations of the whole cluster, as well as of different sub-regions and always found results equivalent to those described below.

The region of the central 1 arcmin contains 192 stars, of which 12, with $V \leq 17$ and $B-V \leq 1.2$, are either BSSs or fore/background objects and cannot be predicted in the synthetic diagrams. By scaling the number of stars detected in the external field (Fig. 3(e)) to the area enclosed in the central 1 arcmin, we can also estimate that 21 of the 192 stars are presumably non cluster members, preferentially distributed along a wide sequence roughly parallel to the MS and overlapping the BSS region. Since the synthetic CMD cannot predict either BSSs or non-member objects, to reproduce the same number of stars as the probable cluster members of the central region, our simulations contain 159 objects.

From the point of view of comparing the CMD morphology, the external stars are few and sparse and therefore only moderately relevant. They may instead affect the luminosity function (LF). To check this effect, we have performed several random selections of the 21/96 stars in the external field and found that their distribution invariably looks sparse and diffuse. At any rate, to take them into account, in the following we compare the observed LF of the central cluster region both to the pure synthetic LFs and to those resulting from the sum of the synthetic stars plus the 12 BSSs and the 21 randomly selected external objects.

Since the data show evidence for a large fraction of binary stars among the cluster members, we have included them in the synthetic diagrams. To do this, a mass ratio has been associated to each system via random extractions from a flat distribution. As for the other clusters, we have followed the prescriptions given by Maeder (1974) to attribute colours and magnitudes to systems with different primary/secondary mass ratios (see Bragaglia et al. 1997 for details). All the stellar models lead to synthetic CMDs in better agreement with the data when the assumed fraction of binaries is 45%; a result in striking agreement with the fraction empirically derived in Sect. 3.2

4.1 Results with FRANEC stellar models

The FRANEC stellar tracks have been recently updated to improve the input physics and include the OPAL opacities (Straniero et al. 1998). Thanks to their authors (Straniero, 1997 private communication), we have been able to use their

new version in advance of publication. Generally speaking, the new models show slightly fainter MS and shorter blue loops (i.e. core He-burning phases in intermediate mass stars) than the older ones. For sake of homogeneity with our previous studies, based on the 1993 FRANEC tracks, we have simulated the CMD of Be21 also with the old set at $Z=0.006$.

The most representative results obtained with the FRANEC stellar models are displayed in Fig. 6, where each row corresponds to the best case resulting from the set of FRANEC tracks indicated in the bottom left corner of that row. The age, reddening and distance modulus corresponding to such cases are listed in Table 5. The three panels in each row show: i) the pure synthetic CMD with 159 stars, on the left; ii) the sum of the latter with the observed CMD of the 12 BSSs candidates and of the 21 probable external objects in the central 1 arcmin (i.e. a total of 192 objects), in the middle; iii) the luminosity functions of the synthetic objects (159, dashed line), of the sum of these stars plus the BSSs and external objects (192, solid line), and of 192 the stars measured in the central 1 arcmin (full dots), on the right.

Panel (d) of Fig. 6 shows one of the synthetic CMDs in better agreement with the data. It is based on the FRANEC98 tracks with $Z=0.006$ and corresponds to: $\tau=2.5$ Gyr, $(m-M)_0=13.6$ and $E(B-V)=0.74$. The two latter values are roughly consistent with the $(m-M)_0=13.9 \pm 0.2$ and the $E(B-V)=0.7 \pm 0.2$ estimated by PJM94 and Janes (1991), respectively. The age is a bit younger, but it is rather difficult to reproduce the cluster features with their value of 2.8 Gyr: the synthetic clump would be too bright, since the older the system, the larger the magnitude difference between TO and clump stars. In fact, with these tracks we obtain a fit of similar quality if we assume an age as young as $\tau=2.3$ Gyr (with $(m-M)_0=13.7$ and $E(B-V)=0.74$).

The LF corresponding to this synthetic CMD is represented by the dashed line in panel (f) of Fig. 6. It shows an apparent paucity of bright stars. However, when the BSSs and the appropriate fraction of field contaminating stars are included (solid line), the resulting LF is consistent with the empirical one (full dots). Notice that we are examining the very central region of the cluster, where paucity of low mass stars with respect to higher mass ones, produced by dynamical evolution and mass segregation, should be in principle more noticeable. In the case of Be21, however, not many of the low mass stars may have been forced to move to the

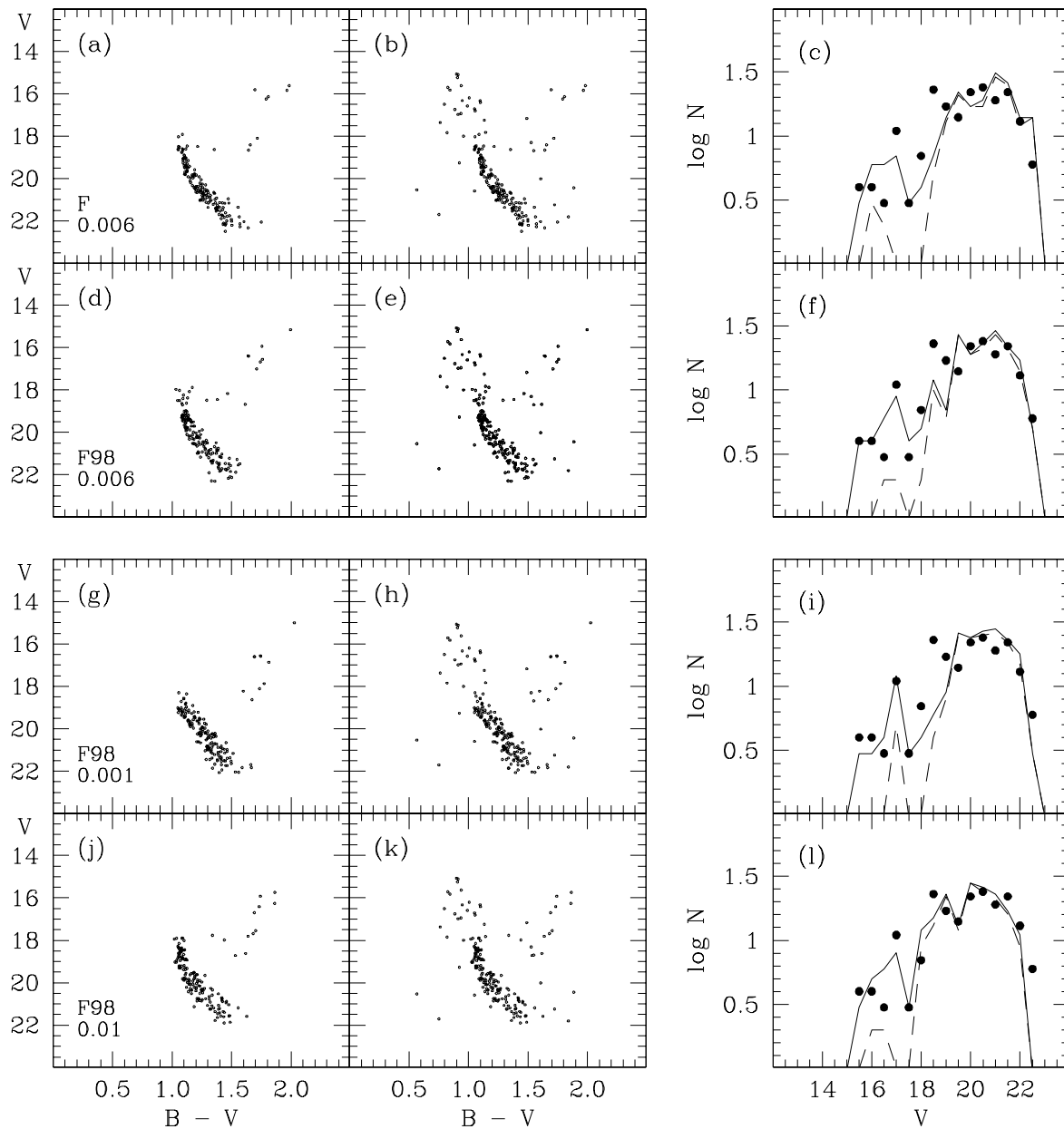


Figure 6. Models in better agreement with the data, for each set of FRANEC tracks (see Tables 4 and 5). Each row shows the synthetic CMD on the left, its superposition to the CMD of 12 BSSs and 21 external objects (see text for details) in the middle, and the comparison of the two corresponding LFs on the right (full dots for observational data points, dashed line for pure synthetic ones, solid line for the latter plus BSSs and external objects). The metallicity is indicated in the bottom left corner of each row.

outermost regions. In fact, the agreement between synthetic and empirical LF at the faintest mag bins shows that Be21 has not lost an appreciable fraction of its lowest mass stars, contrary to other clusters of similar age, but located in inner Galactic regions (e.g. NGC6253, Bragaglia et al. 1997).

The top row in Fig. 6 shows the best case resulting from the old FRANEC tracks with $Z=0.006$. It assumes $\tau=2.3$ Gyr, $(m-M)_0=13.7$ and $E(B-V)=0.78$, i.e., similar age and distance as with the new FRANEC tracks, but slightly higher reddening. The reddening difference is due to the fact that the old tracks are slightly bluer than the new ones, possibly because of the different adopted opacities

and input physics that somehow mimic a lower metallicity (Cassisi et al. 1994). The SGB shows here a larger colour extension (leading also to a too red position of the RGB) than with the FRANEC98 models, and this is probably related to the above effects as well.

Since spectroscopic measurements of stars in Be21 (FJ93) have provided $[\text{Fe}/\text{H}]=-0.97$, corresponding to $Z \approx 0.002$, one would expect to obtain a better reproduction of the observed CMD and LF by adopting the set of tracks with lower metallicity, $Z=0.001$. However, this is not the case for Be21, due to the fact that lower metallicity models have bluer MS and more extended SGB. The intrinsically bluer

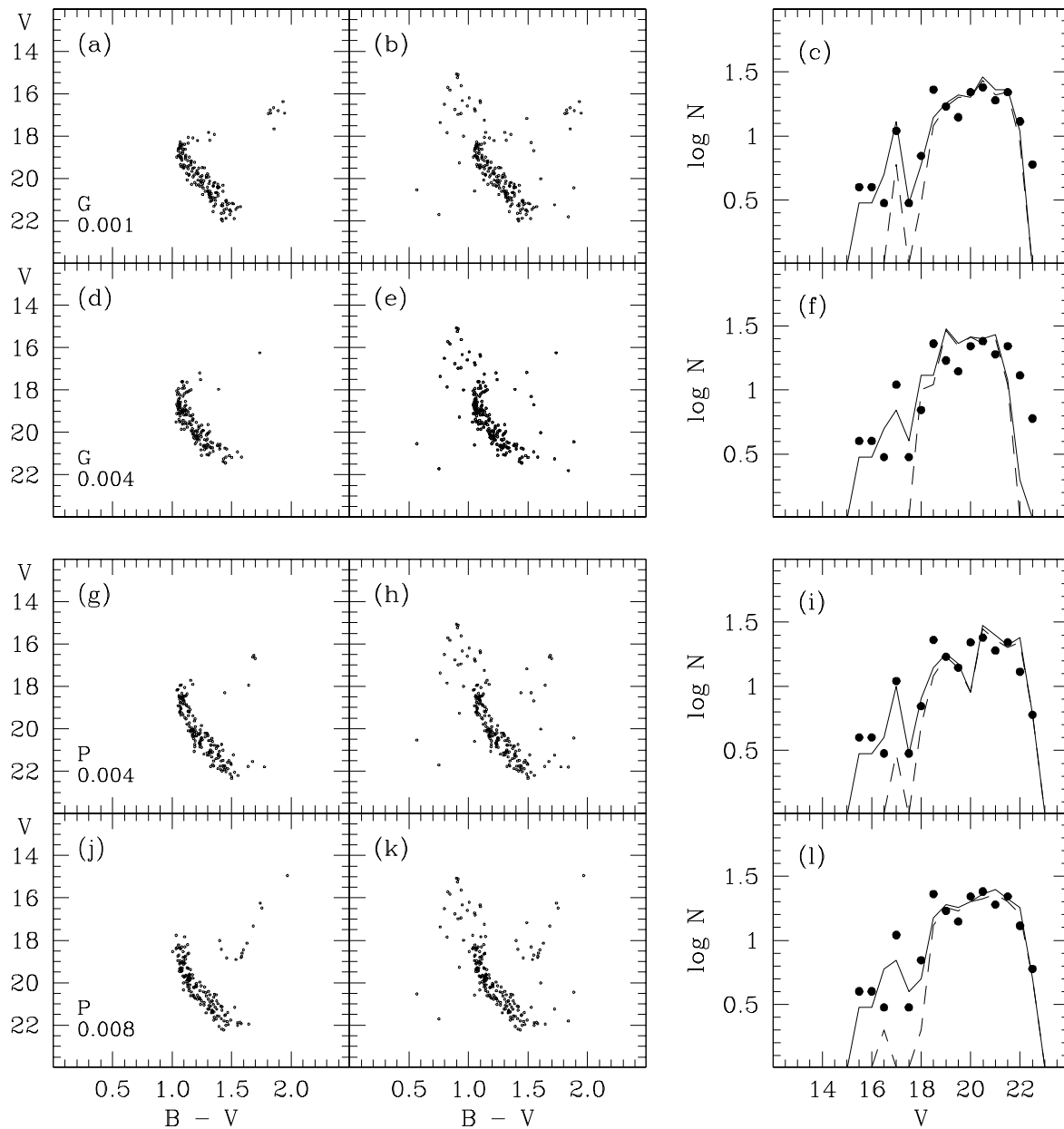


Figure 7. Models in better agreement with the data, for the Geneva (two top rows) and Padova (two bottom rows) sets of tracks (see Tables 4 and 5). Each row shows the synthetic CMD on the left, its superposition to the CMD of 12 BSSs and 21 external objects (see text for details) in the middle, and the comparison of the two corresponding LFs on the right (full dots for observational data points, dashed line for pure synthetic ones, solid line for the latter plus BSSs and external objects). The metallicity is indicated in the bottom left corner of each row.

MS needs fairly high values ($0.8 \lesssim E(B-V) \lesssim 1.0$) for the reddening, to properly fit the observational MS. These reddenings are roughly consistent with that derived by Janes (1991), but, when combined with the large SGB extension, imply RGBs much redder than observed. These problems with the SGB and RGB make the synthetic CMDs with $Z=0.001$ in poor agreement with the data, unless a quite old age (~ 4 Gyr) is assumed for the cluster, in which case the SGB obviously shrinks and the RGB goes back to the appropriate position. Unfortunately, such old ages inevitably imply clumps much brighter than observed and are

therefore unacceptable. In the third row of Fig. 6 we show the best compromise for CMD (and LF) obtained with the FRANEC98 tracks with $Z=0.001$. It assumes $\tau=2.8$ Gyr, $(m-M)_0=13.4$ and $E(B-V)=0.93$. Notice that, in addition to the above problems, the straight shape of the bright MS does not reproduce satisfactorily the observed MS either. We thus exclude that this set of stellar models be appropriate for Be21.

To further verify what is the extent of the metallicity effect on the cluster parameters derived with this method, we have also simulated the observed CMD with the FRANEC98

Table 5. Summary of best-fits results for distance modulus, age, and reddening for each set of stellar models. The FRANEC98 $Z=0.01$ models are interpolated between $Z=0.006$ and $Z=0.02$

Model	Z	(m-M) ₀	τ (Gyr)	E(B-V)
FRANEC	0.006	13.7	2.3	0.74
FRANEC98	0.001	13.4	2.8	0.93
FRANEC98	0.006	13.6	2.5	0.74
FRANEC98	0.010	13.7	1.5	0.76
Geneva	0.001	13.4	2.1	0.97
Geneva	0.004	13.4	2.1	0.60
Padova	0.004	13.5	2.2	0.78
Padova	0.008	13.7	2.3	0.70

tracks with $Z=0.01$, obtained (Straniero 1997, private communication) by interpolating between $Z=0.006$ and $Z=0.02$. This metallicity is admittedly too high, when compared with that spectroscopically derived, but it has been found in several other occasions (e.g. Cassisi et al. 1994, Greggio et al. 1998) that the nominal metallicity of stellar models does not always coincides with the actual one. We thus consider it worthy to use also this set, despite its formally high Z . Unfortunately, the colour extension of the SGB remains too large while the luminosity of the RGB clump becomes significantly higher (probably as a consequence of the higher helium content) and we are forced to select models with quite younger ages to keep the clump at a magnitude level consistent with the data. The bottom row of Fig. 6 shows the best case with $Z=0.01$, corresponding to $\tau=1.5$ Gyr, $(m-M)_0=13.7$ and $E(B-V)=0.76$.

4.2 Results with Geneva stellar models

The Geneva tracks presumably most appropriate for the metallicity of Be21 are those with $Z=0.001$ and with $Z=0.004$. Unfortunately the core-He-burning phase of low mass stars, corresponding to the clump, is not available for the latter, and no direct comparison with this observed feature is thus feasible.

The second row of Fig. 7 shows one of the synthetic CMDs with $Z=0.004$ in better agreement with the data, although definitely not satisfactory. It corresponds to $\tau=2.1$ Gyr, $(m-M)_0=13.4$ and $E(B-V)=0.6$. The lack of He-burning low-mass models, leading to the absence of synthetic stars in the clump phase, prevents any further check on the self-consistency of these values. However, the shape of the MS (which is quite round in this case, but becomes too straight for younger ages and too curved for older ones) and the relative number of objects in the various evolutionary phases limit quite strongly the possible range of ages attributable to Be21 with this set of tracks and, consequently, the corresponding reddening and distance. In other words, even without the clump, we are confident that the cluster parameters derived with this set of models cannot differ significantly from these values.

The Geneva models with $Z=0.001$ do have the clump, allowing more strict constraints on the distance of the cluster. Besides, their metallicity is nominally closer to that spectroscopically determined for the cluster. Nonetheless, the fit to the observational data is much poorer than with

the $Z=0.004$ tracks, due to the excessive colour extent of the subgiant branch, usually attributable to an insufficient metal content. In the best (less bad) case, shown in the top row of Fig. 7, we derive: $\tau=2.1$ Gyr, $(m-M)_0=13.4$ and $E(B-V)=0.97$. The inadequacy of these tracks is also apparent from the very high reddening required to compensate the excessive blueness of their MS. As already mentioned for the FRANEC models, this problem may be attributed to an insufficient metallicity but, possibly, also to details in the input physics which may mimic a different metal content. This latter possibility is suggested by the circumstance that the same set of Geneva stellar models with $Z=0.001$ reproduces quite well the CMD and the LF of the stars in the post-starburst galaxy NGC 1569 (Greggio et al. 1998), whose metallicity, as derived from HII region spectroscopic measurements, is $Z=0.004$. Despite the different mass range of the stars visible in the two systems (massive stars in NGC 1569 and low mass stars in Be 21), we consider it rather improbable that the same set of tracks be simultaneously too metal rich in the massive star range and too metal poor in the low mass range.

4.3 Results with Padova stellar models

The third row of Fig. 7, shows one of the best synthetic CMD resulting from the Padova tracks with $Z=0.004$; it provides $\tau=2.2$ Gyr, $(m-M)_0=13.5$ and $E(B-V)=0.78$. The corresponding LF, once implemented with the BSSs and the appropriate fraction of field contaminating stars, is in agreement with the data, showing that the relative timescales of the various evolutionary phases are well reproduced by these tracks and that this cluster has not suffered any significant loss of stars. This is possibly the best model out of all our simulations based on any stellar evolution set.

Since the cluster features are all rather well reproduced by these tracks, the choice of the age (and therefore of the distance and reddening) is in this case more restrictive than with the other sets, due to the characteristics of the clump luminosity and of the SGB extension. Had we assumed a slightly younger age (e.g. 2 Gyr), the SGB would have turned out too extended in colour and the RGB would have been much too red. Had we instead assumed a slightly older age (e.g. 2.3 Gyr), the clump would have been too bright, due to the larger magnitude difference between TO and clump. For ages older than 2.4 Gyr, also the fit to the MS worsens because its shape becomes too round with respect to the observed one.

It is worth emphasizing that these best fitting models with $Z=0.004$, provide age and distance in agreement with the values derived from the Geneva tracks of same Z (see Table 5). The two derived reddenings are instead quite different. This is due to actual discrepancies in the predictions of the adopted stellar models, and cannot be ascribed to differences in the transformation from the theoretical to the observational plane. In fact, contrary to what is usually done, our procedure consists in adopting the theoretical stellar evolution tracks and transform their $\log L$ and $\log T_e$ into M_V and $B-V$ by using for all sets the same conversion tables. The possible discrepancies between different stellar tracks explain why we consider of fundamental importance to always compare the observational CMDs with more than

one set of stellar models, to have at least an estimate of the corresponding uncertainties.

We have also created synthetic CMDs based on the Padova models with $Z=0.008$, but their fits are worse than those with $Z=0.004$. Rather, with $Z=0.008$ the SGB is almost as extended in colour and much more populated (i.e. with longer relative lifetimes) and, therefore, less consistent with the observed CMD of Be21. This is visible in the bottom row of Fig. 7 where the model with $\tau=2.3$ Gyr, $(m-M)_0=13.7$ and $E(B-V)=0.7$ is shown: the SGB and faint RGB are excessively populated.

Using Padova tracks with metallicity lower than $Z=0.004$, we would find again SGBs with excessive colour extents and quite high required reddenings, as already found for the other sets from FRANEC and Geneva.

5 SUMMARY AND DISCUSSION

Although the fits of observed and simulated diagrams are not as satisfying for Be21 as they have been for other systems examined with the same method, we have been able to determine a fairly consistent confidence interval for its distance, age, reddening and metallicity (see Table 5) by selecting the most reliable among the models described in the previous section. They place it among the old metal poor open clusters, in a region far from the Galactic centre and of moderately high reddening.

5.1 Distance and reddening

We have derived a distance slightly smaller than previous studies, while our evaluation of the reddening is fairly consistent with past works. No previous indication of differential reddening was given in the literature, but our data definitely show it.

JP94 found, for the red clumps of 23 open clusters with $\delta V \geq 1.0$ (i.e. older than about 1.5 Gyr) a mean absolute magnitude $M_V = 0.9 \pm 0.4$, and a mean intrinsic colour $(B-V) = 0.95 \pm 0.10$. In our case, these mean values, when applied to the observed $V=16.80$ and $B-V=1.55$, would imply $(m-M)_V=15.90$, and $E(B-V)=0.60$, or $(m-M)_0=14.04$. From our best simulations, we obtain instead $(m-M)_0 \simeq 13.5$, $E(B-V)=0.76$, corresponding to $(m-M)_V=15.86$. In other words, the clump-based distances seem to agree, but the colour of the clump stars seems to be quite different from the mean. Part of this discrepancy may be due to the high reddening affecting Be21, whose differential effect on blue and red stars leads to an apparent shrink by 0.04 of the true colour difference between TO and clump stars (Fernie 1963, Twarog 1998 private communication). On the other side, TAAT97, derive a mean $M_V = 0.6 \pm 0.1$ for ten clusters not too metal-rich ranging from NGC7789 to Mel66, i.e. approximately from 1 to 5 Gyr, for which they try to measure the distance in a quite homogenous way. This translates, in our case, to $(m-M)_V=16.2$; since they do not cite a mean intrinsic $(B-V)$ no further comparison with our best choice for the reddening is possible.

There are no completely reliable reddening determination for this cluster since the UBV data of CJ do not reach the MS, but our determination and that by Janes (1991) agree well. We have further compared our finding with what

is expected from the spatial distribution of interstellar extinction near the Galactic plane. To this end we have considered the studies of FitzGerald (1968, fig. 3h) and Neckel & Klare (1980, fig. 6i). In both cases, a reasonable estimate deduced from their data for low Galactic latitudes and the right longitude, is $E(B-V) \sim 0.8$; FitzGerald's (1968) observations also allow for a lower value, closer to 0.5, but seem to exclude the high values, close to 1, needed by the lower metallicity tracks of any group.

Janes (1991) and JPM94 give a distance modulus $(m-M)_0=13.9 \pm 0.2$, somewhat larger than our results for every set of tracks. Carraro et al. (1998), working on the same data, cite a Galactocentric distance of 14.5 Kpc, also implying a distance modulus $(m-M)_0 \simeq 13.9$. We have no good explanation for this difference, but we must emphasize that adopting $(m-M)_0=13.9$ we would be forced to select younger ages, and this would have two major drawbacks: a worse disagreement with literature ages (see next), and a worse reproduction of the MS shape in the synthetic CMDs.

5.2 Age

Also in the case of the age, we seem to have found a value lower than given in literature. We can explain the discrepancy partly by the different techniques adopted, partly by the better quality of our data. The various parameter combinations all converge to a fairly small range of possible ages (2.1 to 2.8 Gyr, with favorite age around 2.2 Gyr). In fact, the only largely discrepant value found in our analysis is for the FRANEC98 $Z=0.01$ tracks, a value in strong disagreement with the spectroscopically determined metallicity. Despite the uncertainties involved in the age determination with our method, we consider it still more reliable than ages derived by other means.

Nonetheless, it is not always feasible to determine the age of a cluster with the proper method of synthetic diagram fitting: to do so, high quality data, both deep and precise, are needed, and the process itself is complex. To apply this technique to all the objects of interest takes a long time, while the properties of the whole sample of open clusters are needed to study the Disc population and evolution. For this reason, several parameterizations of cluster ages, based on a handful of well studied objects, have been proposed. These methods, if uncertain in absolute value for the single cluster, yield a reasonable age ranking for the cluster system.

These parameterizations are usually based on a difference, in magnitude and/or in colour, between well recognizable points of the CMD (usually the TO and the red clump), as this is much easier to measure than any absolute quantity. Note though that the precise definition of the two points, and especially of the TO, changes among authors. We will cite here the three following examples: i) Anthony-Twarog & Twarog (1985 and later works) use the magnitude difference between the red giant clump and *the brightest point at the TO* (δV_T) coupled with the difference in colour between the red giant branch at the position of the clump and the bluest point of the TO ($\delta(B-V)_T$); ii) JP94 use a similar δV , but measured between the red clump and *the inflection point between the MS TO and the base of the giant branch*; iii) CC94 define their ΔV as JP94, but assume that *the reference TO luminosity is 0.25 mag fainter than observed in the CMD*, to take into account the fact that presence

Table 6. Comparison of ages for our sample of old clusters derived: by ourselves (col. 2), from the MAI (JP94, col. 4, using δV in col. 3) and from CC94 (or Carraro et al. 1998 when indicated, using either the ΔV in col. 5 or direct analysis). The MAR is given in col. 9 and is derived from δV_T and $\delta(B - V)_T$ (col. 7 and 8); the actual age value depends on the adopted calibration. Also given are the parameters for Be17, considered the oldest open cluster of our Galaxy (Pheps 1997).

Cluster	τ (Gyr)	δV (mag)	MAI (Gyr)	ΔV (mag)	CC94 (Gyr)	δV_T (mag)	$\delta(B - V)_T$	MAR	Notes
Be21	2.2	1.8	2.8		3.1	1.20	0.62	1.94	Carraro et al. 1998
Cr261	7.0	2.6	9.5		7.0	2.56	0.73	3.51	
NGC2243	5.0	2.2	5.6	2.15	4.5	2.00	0.62	3.61	red clump: used brighter part
NGC6253	3.0	2.0	4.4			1.80	0.63	2.86	
NGC2506	1.6	1.5	2.5	1.75	1.9	1.20	0.68	1.76	
Be17	12^{+1}_{-2}	2.7-2.8	10.9-12.6		9.0				Carraro et al. 1998

of unresolved binaries tends to brighten the TO region. In the case of Be21, we have: $\delta V=1.8$ (our measure), $\delta V_T=1.2$, $\delta V(\text{JP94})=1.6$, $\Delta V=1.55$. All these different definitions try to circumvent the problem that the TO point is not always easily identified in open clusters, due to field stars and binaries contamination and/or paucity of stars. The strength of our kind of analysis is that we do not judge on the basis of the observed CMD alone: we know from the tracks the exact location of the TO in each of our simulated CMDs. Given this, we have chosen to measure the magnitude difference as defined above at what we believe to be the true TO, i.e. at the point corresponding to the hottest MS point in the evolutionary tracks.

JP94 correlated δV with cluster ages. The calibration of their Morphological Age Index (MAI, expressed in Gyr) translates for Be21 to an age of 2.8 Gyr (based upon $\delta V=1.6$, PJM94), marginally inconsistent with what we get from the direct comparison with evolutionary tracks (see Section 4). The age difference does not arise from any discrepancy in the two sets of data: we find $\delta V=1.8$, quite consistent with the value given by PJM94 considering that we measure it in a slightly different way. However, we have found in the past (e.g. in the case of NGC2506, Marconi et al. 1997) that the MAI tends to overestimate ages.

Anthony-Twarog & Twarog (1985, revised by Twarog & Anthony-Twarog 1989) proposed the so called Morphological Age Ratio (MAR), defined as $\text{MAR} = \delta V_T / \delta(B - V)_T$ (see above). This index is independent of reddening and almost independent of metallicity (Anthony-Twarog & Twarog 1985, Buonanno et al. 1989). The calibration of the relation between MAR and ages has changed from: age = $1.4 \times \text{MAR}$ Gyr (Anthony-Twarog & Twarog 1985) to: age = $2.0 \times \text{MAR}$ Gyr (Twarog & Anthony-Twarog 1989). Applying their definition to our CMD, we find the values given in Table 6, and an age of about 2.7 to 3.9 Gyr, depending on the adopted calibration. With no attempt to give a new calibration of the MAR-age relation, simply adopting for the clusters we studied the parameters and ages in Table 6, we find: age = $2.3 \times \text{MAR} - 2.6$ (*r.m.s.* = 0.9). We did not include Be17 in this computation: it represents an extreme of the interpolation and we felt that the parameters derived from the published diagrams were too insecure. This relation gives for Be21 an age of 1.9 Gyr.

Carraro et al. (1998) derive for Be21 an age of 3.1 Gyr,

based on the PJM94 data and the synthetic CMD method using the Padova tracks. The difference with our results, obtained employing the same sets of tracks (although we do not interpolate in metallicity as they do), may perhaps be explained simply with the worse quality of the observational data they use. Certainly, in no case are we able to reach self-consistently such a large age.

5.3 Metallicity

We note that our method is unable to solve the problem of the cluster precise metal abundance. The comparison with evolutionary tracks can only give a coarse indication of metallicity. Too many variables are present in tracks computation to discriminate metallicity to such an extent. In fact, tracks nominally closer to the metallicity derived for Be21 from spectroscopic measurements ($[\text{Fe}/\text{H}]=-0.97$, or $Z \simeq 0.002$, FJ93) appear less consistent with the observed CMD than tracks more metal rich, because of the large colour extent of the subgiant branch and, in some cases, of an excessively high reddening required to reproduce the observed colour of the MS.

Anyway, what can be said is that the best fits are obtained for the slightly more metal-rich combinations, i.e. for $Z=0.006$ ($[\text{Fe}/\text{H}]\simeq -0.5$) or 0.004 ($[\text{Fe}/\text{H}]\simeq -0.7$) as compared to 0.001 ($[\text{Fe}/\text{H}]\simeq -1.3$). This would go in favour of a metal abundance slightly higher than measured by FJ93.

There is the possibility that the FJ93 scale may be underestimating cluster metallicities. TAAT97 compared it with abundances based on DDO photometry and found the FJ93 values systematically low. Another example may be the couple of clusters examined by Gratton & Contarini (1994): they observed two giants in each cluster at high-resolution and high S/N ($R=30,000$, $S/N \simeq 100$) and found for NGC2243 and Mel66 the values $[\text{Fe}/\text{H}]=-0.48$ and -0.38 respectively, to be compared with $[\text{Fe}/\text{H}]=-0.56$ and -0.51 (FJ93).

FJ93 emphasized the fact that the actual value derived for the cluster metallicity from their spectra is strongly dependent on the adopted reddening: the ± 0.2 mag error on reddening in Janes (1991) allows for a formal uncertainty of ± 0.3 dex in metallicity. They also find marginal support for a $E(B-V)$ value on the higher side, hence for a metal abundance slightly higher than the $[\text{Fe}/\text{H}]=-0.97$ they give. This

goes in the same direction suggested by our comparisons, even if we do not find any convincing evidence for a larger reddening. Finally, we have identified the four stars studied by FJ93 ($N_{CJ} = 50, 406, 413, 415a$, which correspond to $N_{our} = 50, 67, 20, 51$ respectively), to check if they may be influenced by the differential reddening we found; but we consider it quite improbable, since all the four objects are within 1 arcmin from the centre of the cluster.

No conclusive word can be said on Be21 metallicity, which would instead be important to know with high precision, since it could represent the lowest value for the open clusters in our Galaxy. A decisive answer would come from high resolution spectroscopy coupled with fine abundance analysis on the four stars examined by FJ93, already known to be cluster members.

ACKNOWLEDGEMENTS

We warmly thank A. Chieffi, M. Limongi and, specially, O. Straniero for having not only distributed the new FRANEC tracks in advance of publication, but even in format suitable for our purposes. We also thank J.C. Mermilliod for kindly making available his invaluable BDA open clusters database and for useful comments. We are grateful to the referee (Bruce Twarog) for his comments, extremely useful both to improve the clarity of the paper and for future applications. The bulk of the numerical code for CMD simulations has been provided by Laura Greggio. This research has made use of the Simbad database, operated at CDS, Strasbourg, France.

REFERENCES

- Alongi, M., Bertelli, G., Bressan, A., Chiosi, C., Fagotto, F., Greggio, L., Nasi, E. 1993, *A&AS*, 97, 851
 Anthony-Twarog, B.J., Twarog, B.A. 1985, *ApJ*, 291, 595
 Bonifazi, A., Fusi Pecci, F., Romeo, G., Tosi, M. 1990, *MNRAS*, 245, 15
 Bragaglia, A., Tessicini, G., Tosi, M., Marconi, G., Munari, U. 1997, *MNRAS*, 284, 477
 Buonanno, R., Corsi, C.E., Fusi Pecci, F. 1989, *A&A*, 216, 80
 Carraro, G., Chiosi, C. 1994, *A&A*, 287, 761 (CC94)
 Carraro, G., Ng, Y.K., Portinari, L. 1998, *MNRAS*, in press
 Cassisi, S., Castellani, V., Salaris, M., Straniero, O. 1994, *A&A* 282, 760
 Castellani, V., Chieffi, A. & Straniero, O. 1993, *ApJS* 78, 517
 Charbonnel, C., Meynet, G., Maeder, A., Schaller, G., Schaerer, D. 1993, *A&AS*, 101, 415
 Charbonnel, C., Meynet, G., Maeder, A., Schaerer, D. 1996, *A&AS* 115, 339
 Christian, C.A., Janes, K.A. 1979, *AJ*, 84, 204 (CJ)
 Fagotto, F., Bressan, A., Bertelli, G., Chiosi, C. 1994, *A&AS*, 105, 29
 FitzGerald, M.P. 1968, *AJ*, 73, 983
 Fernie, J.D. 1963, *AJ*, 68, 780
 Friel, E.D. 1995, *ARAA*, 33, 381
 Friel, E.D., Janes, K.A. 1993, *A&A*, 267, 75 (FJ93)
 Gozzoli, E., Tosi, M., Marconi, G., Bragaglia, A. 1996, *MNRAS*, 283, 66
 Gratton, R.G., Contarini, C. 1994, *A&A*, 283, 911
 Greggio, L., Tosi, M., Clampin, M., DeMarchi, G., Leitherer, C., Nota, A., Sirianni, M., 1998, *ApJ*, in press
 Janes, K.A. 1991, *A.G.D. Philip, A.R. Uggren, K.A. Janes, eds*
 Precision photometry: astrophysics of the Galaxy, L. Davis Press (Schenectady USA), p.233
 Janes, K.A., Phelps, R.L. 1994, *AJ*, 108, 1773 (JP94)
 Landolt, A.U. 1992, *AJ*, 104, 340
 Maeder, A., 1974, *A&A*, 32, 177
 Marconi, G., Hamilton, D., Tosi, M., Bragaglia, A. 1997, *MNRAS*, 291, 763
 Neckel, Th., Klare, G. 1980, *A&AS*, 42, 251
 Phelps, R.L. 1997, *ApJ*, 483, 826
 Phelps, R.L., Janes, K.A., Montgomery, K.A. 1994, *AJ*, 107, 1079 (PJM94)
 Schaller, G., Schaerer, D., Meynet, G., Maeder, A., 1992, *A&AS* 96, 269
 Stetson, P.B. 1992, User's Manual for DAOPHOT-II
 Straniero, O., et al. 1988, in preparation
 Tosi, M., Greggio, L., Marconi, G., Focardi, P. 1991, *AJ*, 102, 951
 Twarog, B.A., Anthony-Twarog, B.J. 1989, *AJ*, 97, 759
 Twarog, B.A., Ashman, K.M., Anthony-Twarog, B.J. 1997, *AJ*, 114, 2556 (TAAT97)